



OPEN

The dipole moment of the spin density as a local indicator for phase transitions

SUBJECT AREAS:

NANOPARTICLES
MAGNETIC PROPERTIES AND
MATERIALSD. Schmitz¹, C. Schmitz-Antoniak^{2*}, A. Warland², M. Darbandi^{2†}, S. Haldar³, S. Bhandary³, O. Eriksson³,
B. Sanyal³ & H. Wende²Received
21 March 2014Accepted
2 July 2014Published
21 July 2014Correspondence and
requests for materials
should be addressed to
D.S. (schmitz@
helmholtz-berlin.de)* Current address:
Peter Grünberg Institut
(PGI-6),
Forschungszentrum
Jülich, 52425 Jülich,
Germany.† Current address:
Department of Physics
and Astronomy,
Vanderbilt University,
Station B #351807,
2301 Vanderbilt
Place, Nashville, TN
37235-1807, USA.¹Helmholtz-Zentrum Berlin für Materialien und Energie, Albert-Einstein-Straße 15, D-12489 Berlin, Germany, ²Fakultät für Physik und Center for Nanointegration Duisburg-Essen (CENIDE), Universität Duisburg-Essen, Lotharstr. 1, D-47048 Duisburg, Germany, ³Division of Materials Theory, Department of Physics and Astronomy, Uppsala University, Box-516, SE 75120 Uppsala, Sweden.

The intra-atomic magnetic dipole moment - frequently called $\langle T_z \rangle$ term - plays an important role in the determination of spin magnetic moments by x-ray absorption spectroscopy for systems with nonspherical spin density distributions. In this work, we present the dipole moment as a sensitive monitor to changes in the electronic structure in the vicinity of a phase transition. In particular, we studied the dipole moment at the Fe^{2+} and Fe^{3+} sites of magnetite as an indicator for the Verwey transition by a combination of x-ray magnetic circular dichroism and density functional theory. Our experimental results prove that there exists a local change in the electronic structure at temperatures above the Verwey transition correlated to the known spin reorientation. Furthermore, it is shown that measurement of the dipole moment is a powerful tool to observe this transition in small magnetite nanoparticles for which it is usually screened by blocking effects in classical magnetometry.

X-ray absorption near edge spectroscopy (XANES) and its associated magnetic circular dichroism (XMCD) is an experimental technique that allows for the determination of magnetic properties element-specifically. Today, it is widely spread as one main advantage of XMCD that the orbital moment and the spin moment can be determined independently from each other using sum rules^{1,2} which have been experimentally confirmed for the $3d$ transition metals³. The intra-atomic magnetic dipole moment of the $3d$ spin-density distribution is one term in the XMCD sum rule for the spin moment. More precisely, with the spin sum rule the effective spin moment ($\mu_{S,eff}$), which is the sum of the intrinsic spin moment ($-2 \langle S_z \rangle \mu_B$) and the dipole moment ($7 \langle T_z \rangle \mu_B$) of the spin density distribution, can be determined from the integrals of the XMCD spectrum and the isotropic absorption spectrum². Since the sum rule contains two terms, the contributions of the intrinsic spin moment and the magnetic dipole moment cannot be readily determined. The latter is known to be negligibly small for cubic symmetry only². Limitations of the spin sum rule and the importance of the magnetic dipole term in noncubic environments such as surfaces and interfaces were studied with electronic band structure calculations for iron, cobalt and nickel⁴. The separate determination of spin and magnetic dipole moments with an angle averaging spin sum rule was demonstrated theoretically⁵ and experimentally⁶ for a highly anisotropic $3d$ transition metal system where the charge and spin densities were not spherically symmetric. The magnetic dipole moments of single cobalt atoms and nanoparticles (NPs) were quantified by combining the effective spin moment determined from measured XMCD spectra using the spin sum rule with the intrinsic spin moment calculated in the local spin density approximation⁷. According to *ab initio* studies, the $\langle T_z \rangle$ term, in general, cannot be neglected in the spin sum rule for systems with low dimensionalities like monolayers and monatomic wires⁸ and clusters⁹. Anisotropies of the spin density distributions causing large magnetic dipole moments were also investigated in molecules on surfaces like Cu-phthalocyanine on $\text{Ag}(001)$ ¹⁰ and Fe-octaethylporphyrin on $\text{Cu}(001)$ ¹¹.

For many examples, the measured contribution of the magnetic dipole moment can be regarded as a disadvantage of the XMCD impeding the extraction of the spin moment in a straight-forward way. In this work, we employ it as a monitor for changes in the electronic structure as it is caused by phase transitions. In order to show the potential of the XMCD technique, we chose magnetite (Fe_3O_4) as an example because in magnetite the average Fe dipole moment in the low-temperature phase according to our electronic structure calculations is sufficiently large to be reliably quantified with XMCD. In addition, for magnetite XMCD is also site-selective giving the possibility to distinguish between Fe ions at different lattice sites.

Magnetite crystallizes in the inverse spinel structure in a cubic (isometric) crystal system, with the oxide anions arranged in a cubic close-packed lattice while the Fe cations are located on octahedral and tetrahedral lattice sites



in between. In particular, Fe^{3+} occupies the tetrahedral sites (also denoted A sites in the literature) and half of the octahedral sites (B sites), whereas the Fe^{2+} ions are located at the remaining octahedral sites. For a schematic diagram of the monoclinic P2/c unit cell of magnetite containing 56 atoms we refer to Fig. 1 in Ref. [17]. The strongest interaction is the superexchange between Fe^{3+} on octahedral and Fe^{3+} on tetrahedral sites which is negative resulting in an antiparallel orientation of spins of different sublattices.

At low temperatures, magnetite undergoes a phase transition that was discovered in 1939 by Verwey as a rapid change of the electronic conductivity at a certain temperature and was named after him as the Verwey transition (VT). In the original article¹² it was described as “a sudden increase of the resistance at approximately 117 K by a factor of the order 100”. The resistance of a magnetite sample was compared with the one of a sample which was further oxidized and described as “samples containing an excess of Fe_2O_3 show a much smaller jump in the curve at about 120 K or even merely a change in the temperature coefficient”¹². Many years later it was found by heat capacity studies¹³ that with increasing deviation δ in $\text{Fe}_{3-\delta}\text{O}_4$ from ideal magnetite stoichiometry the VT changes from first to second order and that the VT temperature decreases linearly with δ .

The refined determination of the structural changes at the VT based on diffraction measurements^{14,15} initiated several theoretical investigations with modern methods^{16–18}. The most significant structural change connected to the VT was explained in the work of H.-T. Jeng et al.¹⁷. They reported that in the low-temperature monoclinic unit cell, a charge and orbital ordering is related to one of the Fe^{3+} ions on an octahedral lattice site being pulled inwards the cube diagonal of the sub-unit cell yielding a lower energy of the system due to intersite Coulomb attraction with t_{2g} orbitals of three neighboring Fe^{2+} ions.

With resonant x-ray scattering the changes in the structural, charge and orbital order were studied in dependence of the temperature across the VT using certain diffraction peaks to indicate structural, charge or orbital order^{19–21}. The interpretation of the diffraction peaks was discussed and became a controversy.

In a structural study²¹ using high-resolution synchrotron x-ray powder diffraction data of magnetite the charge disproportion found by J. P. Wright et al.¹⁵ was confirmed between the B1 and B2 sites but

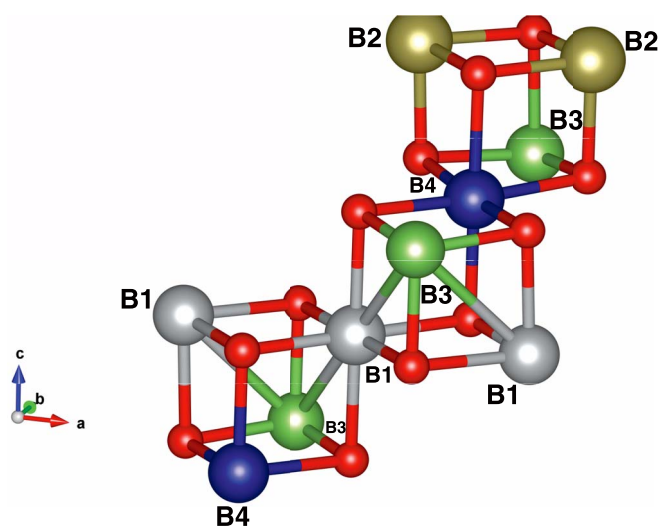


Figure 1 | Part of the magnetite unit cell in the monoclinic crystal structure. Oxygen atoms are drawn as small red spheres. Iron ions on different octahedral sites are drawn as large grey (B1), brown (B2), green (B3) and blue spheres (B4). The linear three-site structure B3–B1–B3 forms a trimeron with reduced B1–B3 bond lengths. The axes of the global coordinate system are also shown.

not between the B3 and B4 sites (see Fig. 1). The picture of a wide distribution of different local environments around the octahedral Fe ions, caused by the condensation of several phonon modes, was favored over any bimodal charge disproportion on the octahedral sites²².

Since diffraction studies of magnetite are hampered by different crystallite orientations and microtwinning, the full low-temperature superstructure has been quite recently determined with x-ray diffraction from an almost single-domain grain of only 40 μm size. There it has also been found that localized electrons are distributed over linear units of three Fe ions on octahedral sites which leads to the observed shortening of the two Fe–Fe distances. These three-Fe-units were viewed as quasiparticles and named “trimerons”²³. More than 30 years earlier the fluctuations of what nowadays is called trimerons were observed above the VT temperature with critical diffuse neutron scattering^{24,25} and interpreted using the Yamada model based on electron-phonon coupling²⁴ and later using a pseudospin-phonon theory²⁵.

Below the VT temperature t_{2g} orbital order on octahedral Fe^{2+} sites has been directly found with resonant soft x-ray diffraction (RSXD)²⁶. For this method it is important to take into account that there is a layer at the surface of single crystals which contributes to the absorption but not to the diffraction of the soft x-rays²⁷. By studying the azimuthal dependence of the diffracted intensity it has been shown that the distortion of the $3d$ orbitals towards monoclinic symmetry is by far larger than that of the lattice²⁸. Ultrafast melting of the charge-orbital order leading to the formation of a transient phase, which had not been observed in equilibrium, was observed with time-resolved RSXD with a free-electron laser²⁹. Very recently it was investigated on the ps time scale how trimerons become mobile across the VT³⁰.

In magnetite NPs the VT has already been experimentally observed with different methods, e.g., magnetization measurements of a non-diluted system containing strong dipolar interparticle interactions³¹ and magnetoresistance measurements of tunneling junctions of stacked monolayers of magnetite NPs of 5.5 nm average diameter for which a VT temperature of 96 K has been determined³². In these studies it has been found that the VT temperature significantly decreases when decreasing the size of the NPs to a small fraction³¹ but that it is not very sensitive to small changes of the order of 10% of the particle size³².

However, one may note that in magnetometry, the VT can only hardly be distinguished from a spin reorientation transition that occurs in magnetite at slightly higher temperatures ($T_{SR} \approx 132 \text{ K}^{33}$). The spin reorientation is characterized by a vanishing magnetocrystalline anisotropy constant K_1 , which is negative at room temperature. With decreasing temperature it decreases, acquiring a minimum at a temperature of about 250 K³⁴. With further decreasing temperature, it increases and becomes positive at T_{SR} . Referring to the vanishing value of K_1 , this temperature is also called *isotropy point* in literature. For single crystalline samples, the different transition temperatures were measured by recording the saturation isothermal remanent magnetization along a principal axis of the single crystal³³. For the case of an arbitrary orientation of the magnetic field with respect to the principal crystallographic axes, the effects of T_{SR} and the VT on the remanence could not be clearly separated. For polycrystalline samples it seems to be impossible to distinguish between the two transitions. As pointed out by Rezníček et al.³⁴, there exists a correlation between the spin reorientation and the VT. In this work, the authors connected the contribution to K_1 which leads to an anomalous increasing behavior with decreasing temperature between 250 K and T_{SR} to a local charge and orbital ordering that becomes long-range and stable for temperatures below the VT.

The main purpose of the present paper is to study the magnetic moments, in particular the magnetic dipole moment of Fe as a function of temperature across the phase transitions in magnetite NPs



with a diameter of 6 nm and a 200 nm thick polycrystalline magnetite film which serves as a reference. For this purpose a combination of experimental and theoretical methods, *i.e.* XANES, XMCD, vibrating sample magnetometry (VSM) and electronic structure calculations based on density functional theory, has been used. As it will be described in detail below, a transition of the dipole moment of the Fe 3d spin-density distribution was experimentally found well above the VT and theoretically explained.

Results

Density functional theory. Calculations of the electronic structure were performed based on density functional theory on cubic (high temperature) and monoclinic (low temperature) structures of magnetite. Details of the calculations are described in the methods section. We have considered a monoclinic P2/c structure with 56 atoms per unit cell obtained by using high-resolution neutron and x-ray powder-diffraction data by Wright *et al.*^{14,15}. A part of the monoclinic unit cell with its four inequivalent octahedral lattice sites, labelled B1–B4, is shown in Fig. 1. The resulting magnetic moments are shown in table I. The Fe sites are named as shown in Fig. 1 and like in Ref. [17]. Our calculated values of $\langle T_z \rangle$ for the cubic structure are negligible ($\sim 10^{-5} \mu_B$) whereas for the monoclinic structure, they are quite large, especially for the octahedral B sites. It is clearly observed from the calculations that the Fe²⁺ ion has a larger contribution than Fe³⁺ (see Table I, where we compile the calculated values of $7 \langle T_z \rangle$). At the B4 site, the contribution is as large as $-1.44 \mu_B$ with an anti-parallel alignment to the spin moment. It is only partly compensated by the second largest contribution of $0.72 \mu_B$ at the B1 site with a parallel alignment to the spin moment. Therefore, these octahedral sites substantially modify the effective spin moments, as detected in the XMCD measurements.

We also calculated the Fe orbital magnetic moments for the monoclinic phase in the *a*, *b* and *c* directions as defined in Fig. 1. The sizeable orbital moments can be as large as $0.035 \mu_B$ along the *c* direction for Fe ions on B4 sites and $0.031 \mu_B$ along the *b* direction for Fe ions on B1 sites. For all other sites, the orbital moments are almost isotropic with absolute values of $0.015 \mu_B$ to $0.019 \mu_B$. The signs of the orbital moments follow the spin moments. To further analyze the large values of $\langle T_z \rangle$, we show in Fig. 2, the m_l projected density of states (DOS) for different octahedral sites of the monoclinic phase. The reason for the high $\langle T_z \rangle$ value is the full occupancy of the $d_{x^2-y^2}$ orbital in the spin down channel of the Fe²⁺ ion on the B4 site. For the Fe³⁺ ion, this orbital is unoccupied. Similarly, a high value (half of that of the B4 site, and with parallel alignment to the spin-moment) is observed for the Fe²⁺ ion on the B1 site. The large value also for this site is coupled to the fact that the d_{xz} and d_{yz} orbitals are occupied, although only partially. Again, for the Fe³⁺ ion, both these orbitals are unoccupied, and do not contribute to $\langle T_z \rangle$.

All of our calculated results can be understood from the $\langle T_z \rangle$ matrix elements explicitly provided in the paper by Crocombette *et al.*³⁵. For Fe³⁺, the spin-up channel is completely filled with almost

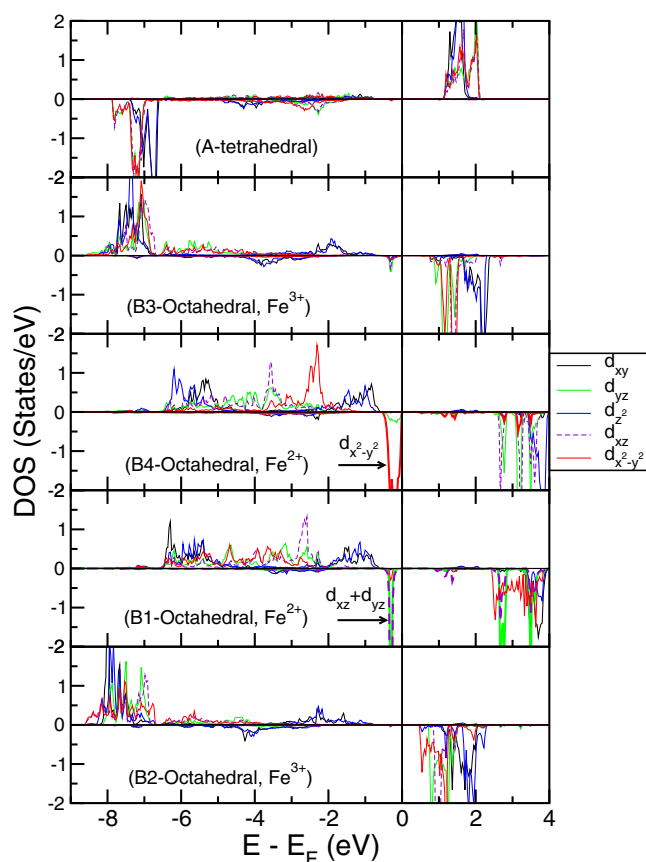


Figure 2 | Spin-resolved m_l projected density of states for the monoclinic structure. DOS at the tetrahedral A site along with four different octahedral B sites are shown. The Fe sites are named as shown in Fig. 1 and like in Ref. [17]. The specific orbitals responsible for the large contribution in the $\langle T_z \rangle$ part are indicated by arrows. The energies in the x-axes are plotted with respect to the Fermi level E_F .

no occupancy in the spin-down channel and therefore, much smaller $\langle T_z \rangle$ contributions are observed. Note that XANES and XMCD are sensitive to the unoccupied DOS so that in these experiments the magnetic moments due to the lack of unoccupied states instead of the existence of occupied states is probed. Also note that even for Fe³⁺ in the monoclinic phase due to the low symmetry structure compared to the cubic one, we have higher contribution to $\langle T_z \rangle$ compared to the cubic one. Obviously, there is no noticeable distinction between Fe²⁺ and Fe³⁺ in the cubic phase as the charge ordering is non-existent in the metallic phase.

X-ray absorption spectroscopy. The XANES and XMCD spectra are defined as the sum and difference of two spectra obtained with opposite helicities of the incident circularly polarized soft x-ray radiation, respectively. Measured XANES spectra and corresponding XMCD spectra of the NPs and the film sample are shown in Fig. 3 and Fig. 4, respectively, at the Fe $L_{2,3}$ absorption edges for various temperatures. The temperature and magnetic field histories of both samples were identical, *i.e.* both samples were field-cooled to 4 K in a magnetic field of 0.5 T and subsequently heated stepwise to and measured at the temperatures indicated by the data points in Fig. 5 in a magnetic field of 3 T. The NPs offer significant changes of the XANES intensity and the XMCD intensity between 50 K and 100 K and the film sample between 150 K and 175 K. For both samples the spectra are divided into two groups: Spectra for temperatures below the change are shown as blue lines, and above as red lines.

XMCD has the advantage that spin and orbital moments can be determined element-specifically by use of sum rules^{1,2}. For the deter-

Table 1 | Charge, spin and magnetic dipole moments for 3d orbitals of Fe atoms at different sites in the monoclinic unit cell. Also, effective moments ($\mu_{S,eff} = -2 \langle S_z \rangle \mu_B + 7 \langle T_z \rangle \mu_B$) are provided. The Fe sites are named as in Ref. [17]

Fe site	d-charge	$-2 \langle S_z \rangle$	$7 \langle T_z \rangle$	$\mu_{S,eff} (\mu_B)$
A1	5.91	-3.98	-0.015	-3.995
A2	5.91	-3.98	0.025	-3.955
B1	6.08	3.67	0.72	4.39
B2	5.82	4.14	0.043	4.183
B3	5.85	4.08	0.027	4.107
B4	6.1	3.64	-1.44	2.20

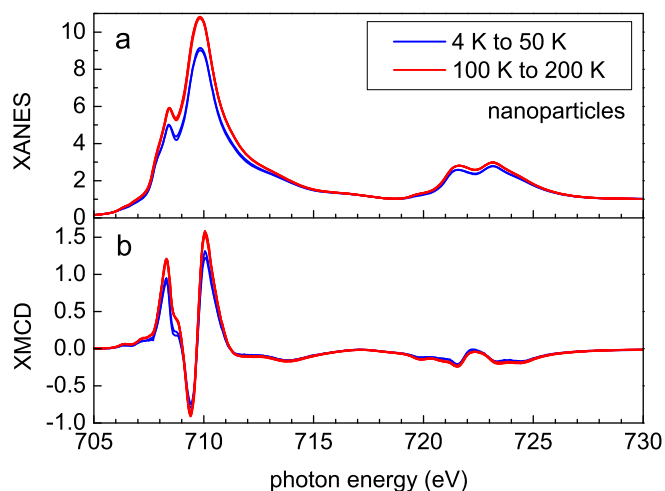


Figure 3 | Measured XANES (a) and corresponding XMCD spectra (b) of the nanoparticles at the $L_{2,3}$ absorption edges. The XANES spectra are shown after subtracting a linear background and normalizing at a photon energy in the post-edge region.

mination of the magnetic moments via sum rules, we normalized the spectra in the usual way, i.e. first subtracted a constant background, then normalized at a photon energy above the absorption edge and finally subtracted a step like function. Please note that the spectra have been measured from 680 eV to 780 eV in order to be able to perform a reliable normalization. In Fig. 3 and Fig. 4 only the physically relevant spectral range from 705 eV to 730 eV has been shown for the sake of clarity. The effective spin moment ($\mu_{S,eff} = -2 \langle S_z \rangle \mu_B + 7 \langle T_z \rangle \mu_B$) is defined as the intrinsic spin moment ($-2 \langle S_z \rangle \mu_B$) plus the magnetic dipole moment ($7 \langle T_z \rangle \mu_B$) of the spin-density distribution² where z is defined by the magnetization direction. Its normalized values determined from the measured XMCD spectra as a function of temperature are shown for the NPs in Fig. 5a and for the film in Fig. 5b. The effective Fe spin moment of the NPs increases between 50 K and 100 K by about 7% relative to the value at 100 K and for the film between 150 K and 175 K by 16% relative to the value at 175 K. The magnetic moments of the NPs and the film sample were also measured with VSM and are shown as gray lines in Fig. 5a and Fig. 5b, respectively. Increases of the

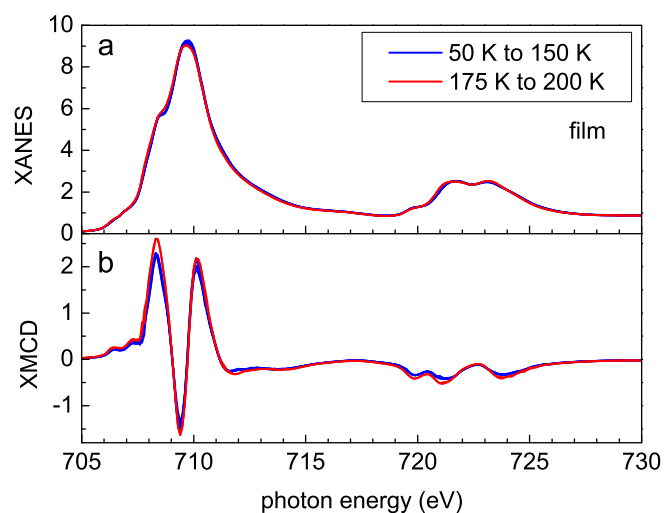


Figure 4 | Measured XANES (a) and corresponding XMCD spectra (b) of the film sample at the $L_{2,3}$ absorption edges. The XANES spectra are shown after subtracting a linear background and normalizing at a photon energy in the post-edge region.

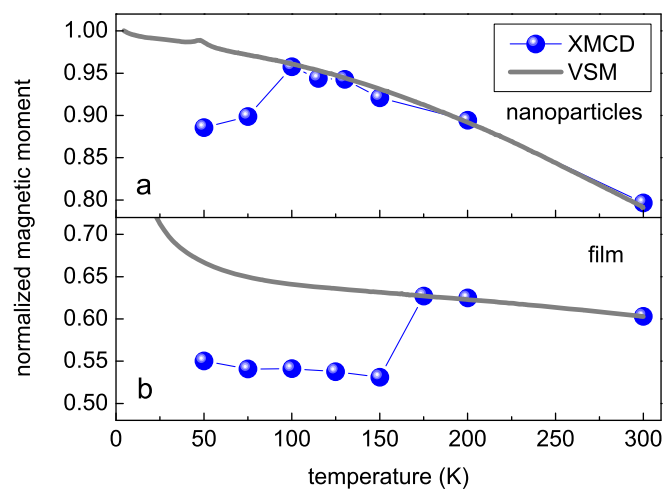


Figure 5 | Normalized effective Fe spin moments as determined from the measured XMCD spectra (solid symbols) and the magnetic moment measured with VSM (thick gray line) as a function of temperature for the magnetite NPs (a) and the film sample (b). Errors due to the reproducibility of the evaluation of the XMCD spectra are within the symbol size.

magnetic moments with increasing temperatures were not observed with VSM. This important result is due to the fact that the magnetic dipole moment is observable with XMCD but not with VSM as discussed in the following section.

Discussion

The electronic structure calculations show a strong change of the magnetic dipole moment in magnetite when the structure of the lattice changed from cubic to monoclinic. These changes are most significant for the case of Fe^{2+} ions on octahedral lattice sites (B1, B4) which is in agreement to the experimental XMCD data. The transition observed with XMCD (Fig. 3b and Fig. 4b) is accompanied by a change of the asymmetry, which is defined as the XMCD spectrum divided by the XANES spectrum after adequate background subtraction and normalization, at the photon energies 708.2 eV and 710 eV which mainly correspond to octahedral sites³⁸. The transition is also observed in the effective Fe spin moment (Fig. 5). However, in general this transition could be assigned to a change in the spin moment, the magnetic dipole moment or both at the same time. To analyse which contribution to the effective spin moment is mainly responsible for its significant change, the XMCD results are compared to magnetometry data obtained with VSM. The $\langle T_z \rangle$ term only shows up in XMCD measurements because they involve an excitation from a core level to an unoccupied valence level. It does not show up in magnetometry or other probes that detect the macroscopic magnetization. For further discussion, see Ref. [39] and Ref. [40]. As shown in Fig. 5, there is no corresponding increase of the total magnetic moment in the VSM data although this method certainly is sufficiently sensitive to detect a change of about 7% for the NPs and 16% for the film. Therefore the transition observed with XMCD cannot be due to a change in the intrinsic Fe spin moment but must be due to a change in the second term of the sum rule for the effective spin moment², i.e. the $\langle T_z \rangle$ term which describes the dipole moment of the Fe spin-density distribution. This conclusion is in accordance with our theoretical treatment of the VT.

In Fig. 6, we compare the experimentally determined values of the effective spin magnetic moment of the NPs with the theoretically observed ones. The calculated 0 K effective moments, averaged over all Fe sites have been multiplied with the Bloch law $1 - 0.96 (T/850\text{K})^{3/2}$ to obtain magnetic moments as a function of temperature. The theoretical moments are seen to drop at the known VT



temperature for the bulk, where the crystal structure changes from cubic to monoclinic. Again, it is the value of $\langle T_z \rangle$ that changes. The relative change of the moments nicely agrees between theory and experiment in particular for the NPs although $\langle T_z \rangle$ was calculated along one crystallographic direction (the c direction as indicated in Fig. 1) whereas in the measurement it was averaged over all directions due to the random orientation of the NPs. Nevertheless, it is clear that a detailed measurement of $\langle T_z \rangle$ shows up in an unprecedented way. This then becomes a valuable characterization tool, that signals not only changes in the local geometry but also the local electronic structure. It is likely that in general, detailed knowledge of $\langle T_z \rangle$ is a valuable tool for understanding local changes in the crystal- and electronic structure, not only for complex oxides but also complex actinide and rare-earth compounds.

For $3d$ transition metals it has been pointed out by Stöhr and König⁵ that spin-orbit correction terms in the perturbative calculation of $\langle T_z \rangle$ can be neglected to a good approximation, leading to the numerical relation $\langle T_x \rangle + \langle T_y \rangle + \langle T_z \rangle \approx 0$ and to the possibility to average out the magnetic dipole moment by magnetizing and measuring the sample along the three cartesian axes ($\alpha = x, y, z$). In the case of our magnetite NPs the average magnetic dipole moment would vanish in each single measurement geometry because the NPs are randomly oriented like in a powder sample so that the integration of the z component $T_z = S_z(1 - 3\cos^2\theta)/2^4$ over the solid angle yields zero. However, according to Ederer *et al.* the effects of spin-orbit coupling are larger for low-dimensional systems⁸ and in particular the relation $\langle T_x \rangle + \langle T_y \rangle + \langle T_z \rangle \approx 0$ is strongly violated for monoatomic Fe, Co and Ni wires⁴¹. In addition, spin-orbit coupling is larger for $3d$ oxides like magnetite than for $3d$ metals due to a stronger localization of the $3d$ electrons. The large spin-orbit coupling becomes noticeable by the large magnetic anisotropy constant in the monoclinic phase of magnetite³⁴. Moreover, it causes that the $3d$ charge distribution is no longer independent from the spin direction⁵. Therefore the effect of spin-orbit coupling in the determination of the components $\langle T_z \rangle$ can no longer be neglected, *i.e.* the terms containing the spin-flip operators do no longer vanish (see Appendix B in Ref. [40]). For the experimental determination of the magnetic dipole moment this means that at least a part of the magnetic dipole moment is fixed to the magnetization direction but not to the crystal lattice when the crystal (here each NP) is rotated relative to the magnetic field. In this case it is not possible to separate the intrinsic spin moment and the magnetic dipole moment solely by angle dependent XMCD measurements because the precondition for averaging out the magnetic dipole moment is no longer fulfilled. The present results for magnetite NPs with 6 nm diameter demonstrate

that the magnetic dipole moment indeed is not averaged out in the monoclinic low-temperature phase.

The small average Fe orbital moments of magnetite with values below $0.03 \pm 0.02 \mu_B$ as determined with XMCD experiments in Ref. [37] do not exclude sizeable local spin-orbit effects because, according to our calculations, the absolute values of the Fe orbital moments vary strongly with the lattice site and their signs follow the spin moments so that they partly cancel each other like the spin moments and magnetic dipole moments do. In addition, the NPs will show higher values of the Fe orbital moments due to surface effects. For the 200 nm thick polycrystalline magnetite film which served as a bulk reference the VT was observed with VSM at 120 K as shown in the Supplementary Information. With field-cooled/zero-field-cooled measurements peaks in the blocking temperature distributions were found at 120 K, which indicate the VT because their temperature positions were independent of the magnitude of small magnetic fields. Interestingly, at this temperature no transition was observed with XMCD in accordance with the results in Ref. [37]. Surprisingly, with XMCD a transition was detected well above the VT temperature, *i.e.* between 150 K and 175 K. An error in the temperature measurement can be excluded because with the used experimental setup, *i.e.* the high-field endstation at beamline UE46-PGM1 at the electron storage ring BESSY II, various transitions between 4 K and 300 K have been found at the known transition temperatures. Therefore we believe that the enhanced absolute values of the magnetic dipole moments of the monoclinic structure persist above the VT temperature until a temperature between 150 K and 175 K. This is in agreement with the unusual temperature dependence of the magnetocrystalline anisotropy that can be explained by a local charge and orbital ordering well above the VT as suggested by Řezníček *et al.*³⁴. In this sense, our work gives the first experimental evidence for this interpretation of changes in the electronic structure above the VT.

For the NPs, the spectral shapes in Fig. 3a and Fig. 3b indicate that a charge transfer could be present to ligands which have not been washed out completely after the synthesis³⁸, or that the NPs are further oxidized at the surface⁴². According to our experience both processes, charge transfer to ligands and oxidation at the surface, result in similar spectra³⁸. However, the transition observed with XMCD disappeared after storing the NPs 17 months in solution. The transition was re-observed with XMCD after treating the NPs *in-situ* with a Hydrogen plasma which resulted in perfect magnetite composition according to the XANES and XMCD spectra. Therefore we confidently associate the transition observed with XMCD with magnetite.

Compared to the film sample, the transition temperature of the NPs is reduced. A reduction of the VT temperature of NPs is known from other experiments with different methods^{26,27} and was explained with spin canting and reduced thermal stability at the surface⁴³. In our NPs, spin canting has also been experimentally observed as a finite slope at high magnetic fields in magnetization hysteresis measurements with XMCD⁴⁴ and with Mössbauer spectroscopy as described in Ref. [45]. Thus, a reduced VT temperature seems to be reasonable and can explain the reduced transition temperature measured with XMCD. For the case of NPs, magnetometry data may not be sufficient to detect changes in the magnetic properties caused by a phase transition, due to a strong influence of blocking effects as discussed in the Supplementary Information where we present VSM data of our NPs. This shows the importance of measurements of the magnetic dipole moment as a sensitive detector for local changes of the electronic structure.

One might ask whether it is reasonable to attribute the observed transition of the magnetic dipole moment to quasiparticles called trimers. Trimers consist of a linear unit of three Fe ions on octahedral sites in which a t_{2g} minority-spin electron from the central Fe^{2+} donor site is distributed over two adjacent Fe^{3+} acceptor

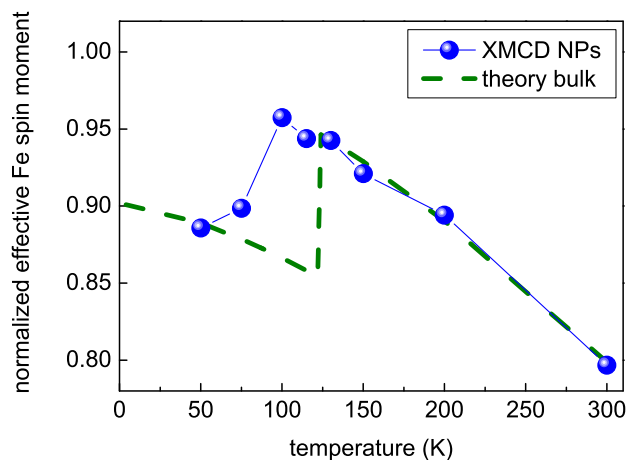


Figure 6 | Normalized experimental effective Fe spin magnetic moments of magnetite NPs (blue symbols) compared to theoretically obtained results (dashed line).



sites²³. This distribution tends to shorten the two corresponding Fe²⁺-Fe³⁺ distances which was recently observed with x-ray scattering²³. Intuitively, one might expect that this donated t_{2g} minority-spin electron creates an anisotropy of the spin density distribution which is accompanied by a magnetic dipole moment. According to our electronic structure calculations the B1–B3 bond length is shorter than other bond lengths in the unit cell which corresponds to B3–B1–B3 trimers as shown in Fig. 1. The first potential donor site, B1 Fe²⁺, is part of a trimeron and its d_{xz} and d_{yz} orbitals exhibit a magnetic dipole moment of $0.72 \mu_B$. Contrary, the second potential donor site, B4 Fe²⁺, which carries the largest magnetic dipole moment of $-1.44 \mu_B$ in its $d_{x^2-y^2}$ orbital, is not part of a trimeron. Therefore it is not sufficient to assign the observed total magnetic dipole moment just to trimerons.

Summary. In summary, magnetite NPs with 6 nm diameter and a 200 nm thick polycrystalline magnetite film which served as a bulk reference were experimentally investigated with XANES, XMCD and VSM and compared with electronic structure calculations based on density functional theory. The measured spectra of the NPs offered significant changes in the white line intensity and the XMCD asymmetry between 50 K and 100 K. The film sample also showed the transition in the XMCD asymmetry which appeared between 150 K and 175 K. A sum rule analysis of the XMCD spectra revealed that the transition observed with XMCD is due to an increase of the effective Fe spin moment with increasing temperature which was attributed to a change of the dipole moment of the Fe $3d$ spin-density distribution. This conclusion was verified and explained with electronic structure calculations based on density functional theory. The large absolute value of the negative magnetic dipole moment in the monoclinic structure is caused by the full occupancy of the $d_{x^2-y^2}$ orbital in the spin down channel of the Fe²⁺ ion on the B4 site resulting in a negative magnetic dipole moment, which is only partly compensated by the positive magnetic dipole moment of partially occupied d_{xz} and d_{yz} orbitals of the Fe²⁺ ion on the B1 site. Since the B1 site but not the B4 site is part of a trimeron it is not meaningful to attribute the observed total magnetic dipole moment just to trimerons. In the case of magnetite, the experimental results evidence the occurrence of local charge and orbital ordering well above the VT as suggested in a recent publication³⁴. In general, detailed knowledge of the magnetic dipole moment is a valuable tool for understanding local changes in the crystal- and electronic structure, not only for complex oxides but also complex actinide and rare-earth compounds.

Methods

Synthesis of nanoparticles. The NPs were prepared using a one-pot water-in-oil microemulsion technique as described in detail elsewhere⁴⁵. FeCl₂ and FeCl₃ were used as precursors, IGEPAL® CO-520 (polyoxyethylene (5) nonylphenylether) as stabilizing organic surfactant and ammonium hydroxide as catalyst. The water droplets coated by the surfactant act as nanoreactors in which the magnetite NPs are formed. The diameters of the NPs (6.3 ± 0.9 nm) were determined with transmission electron microscopy averaging over a few hundred NPs. The NPs were prepared at the University of Duisburg-Essen, transported in liquid solution to Berlin, deposited onto substrates and transferred into ultra-high vacuum for the measurements.

X-ray absorption. The XANES and XMCD measurements were performed in the highfield endstation at beamline UE46-PGM1 with polarized synchrotron radiation from an elliptical undulator in the electron storage ring BESSY II of the Helmholtz-Zentrum Berlin. The total electron yield (TEY) method used in the present measurements to monitor the absorption of the soft x-rays has an information depth which is determined by the mean free path of the secondary photoelectrons of 1 nm to 2 nm. Since the magnetite NPs have a mean radius of 3 nm, the element-specific XANES and XMCD spectra represent the average over the whole particle with a pronounced signal from the surface with respect to the core.

Magnetometry. The VSM measurements were performed with a Physical Properties Measurement System from the company Quantum Design which has a sensitivity of about 10^{-9} J/T and is operated in the laboratory cluster at the Helmholtz-Zentrum Berlin.

Density functional theory. The generalized gradient approximation (GGA) as given by Perdew, Burke and Ernzerhof³⁶ plus on-site Coulomb interaction U to include strong electron correlation in the d -orbitals of Fe were used. The Coulomb parameter $U = 4.5$ eV⁴⁶ and the exchange parameter $J = 0.89$ eV⁴⁷ were used for all Fe- d orbitals. The projector augmented wave method^{48,49} as implemented in plane-wave based density functional code VASP⁵⁰ has been used for the calculations. The plane wave cutoff energy was set at 400 eV energy. $12 \times 12 \times 12$ and $12 \times 12 \times 4$ Monkhorst-Pack k -point grids in the Brillouin zone were used for cubic and monoclinic structures respectively. The geometries were optimized until the force on all each atom was reduced to 0.1 eV/nm.

- Thole, B. T., Carra, P., Sette, F. & van der Laan, G. X-ray circular dichroism as a probe of orbital magnetization. *Phys. Rev. Lett.* **68**, 1943–1946 (1992).
- Carra, P., Thole, B. T., Altarelli, M. & Wang, X. X-ray circular dichroism and local magnetic fields. *Phys. Rev. Lett.* **70**, 694–697 (1993).
- Chen, C. T. *et al.* Experimental confirmation of the x-ray magnetic circular dichroism sum rules for iron and cobalt. *Phys. Rev. Lett.* **75**, 152 (1995).
- Wu, R. & Freeman, A. J. Limitation of the magnetic-circular-dichroism spin sum rule for transition metals and importance of the magnetic dipole term. *Phys. Rev. Lett.* **73**, 1994 (1994).
- Stöhr, J. & König, H. Determination of spin- and orbital-moment anisotropies in transition metals by angle-dependent x-ray magnetic circular dichroism. *Phys. Rev. Lett.* **75**, 3748 (1995).
- Weller, D. *et al.* Microscopic origin of magnetic anisotropy in Au/Co/Au probed with x-ray magnetic circular dichroism. *Phys. Rev. Lett.* **75**, 3752 (1995).
- Gambardella, P. *et al.* Giant magnetic anisotropy of single cobalt atoms and nanoparticles. *Science* **300**, 1130–1133 (2003).
- Ederer, C., Komelj, M. & Fähnle, M. Magnetism in systems with various dimensionalities: A comparison between Fe and Co. *Phys. Rev. B* **68**, 052402 (2003).
- Sipr, O., Minar, J. & Ebert, H. On the importance of the magnetic dipole term T_z in analyzing X-ray magnetic circular dichroism spectra of clusters. *Europhys. Lett.* **87**, 67007 (2009).
- Stepanow, S. *et al.* Giant spin and orbital moment anisotropies of a Cu-phthalocyanine monolayer. *Phys. Rev. B* **82**, 014405 (2010).
- Herper, H. C. *et al.* Iron porphyrin molecules on Cu(001): Influence of adlayers and ligands on the magnetic properties. *Phys. Rev. B* **87**, 174425 (2013).
- Verwey, E. J. W. Electronic conduction of magnetite (Fe₃O₄) and its transition point at low temperatures. *Nature* **364**, 327–328 (1939).
- Shepherd, J. P., Koenitzer, J. W., Aragon, R., Spalek, J. & Honig, J. M. Heat capacity and entropy of nonstoichiometric magnetite Fe_{3(1- δ)}O₄: The thermodynamic nature of the Verwey transition. *Phys. Rev. B* **43**, 8461–8471 (1991).
- Wright, J. P., Attfield, J. P. & Radaelli, P. G. Long range charge ordering in magnetite below the Verwey transition. *Phys. Rev. Lett.* **87**, 266401 (2001).
- Wright, J. P., Attfield, J. P. & Radaelli, P. G. Charge ordered structure of magnetite Fe₃O₄ below the Verwey transition. *Phys. Rev. B* **66**, 214422 (2002).
- Leonov, I., Yaresko, A. N., Antonov, V. N., Korotin, M. A. & Anisimov, V. I. Charge and orbital order in Fe₃O₄. *Phys. Rev. Lett.* **93**, 146404 (2004).
- Jeng, H.-T., Guo, G. Y. & Huang, D. J. Charge-orbital ordering and Verwey transition in magnetite. *Phys. Rev. Lett.* **93**, 156403 (2004).
- Piekarz, P., Parlinski, K. & Oleś, A. M. Mechanism of the Verwey transition in magnetite. *Phys. Rev. Lett.* **97**, 156402 (2006).
- Lorenzo, J. E. *et al.* Charge and orbital correlations at and above the Verwey phase transition in magnetite. *Phys. Rev. Lett.* **101**, 226401 (2008).
- Garcia, J. *et al.* Reexamination of the temperature dependence of resonant reflections in highly stoichiometric magnetite. *Phys. Rev. Lett.* **102**, 176405 (2009).
- Blasco, J., Garcia, J. & Subias, G. Structural transformation in magnetite below the Verwey transition. *Phys. Rev. B* **83**, 104105 (2011).
- Subias, G. *et al.* Structural distortion, charge modulation and local anisotropies in magnetite below the Verwey transition using resonant x-ray scattering. *J. Synchrotron Rad.* **19**, 159–173 (2012).
- Senn, M. S., Wright, J. P. & Attfield, J. P. Charge order and three-site distortions in the Verwey structure of magnetite. *Nature* **481**, 173–176 (2012).
- Fujii, Y., Shirane, G. & Yamada, Y. Study of the 123-K phase transition of magnetite by critical neutron scattering. *Phys. Rev. B* **11**, 2036 (1975).
- Shapiro, S. M., Iizumi, M. & Shirane, G. Neutron scattering study of the diffuse critical scattering with the Verwey transition in magnetite (Fe₃O₄). *Phys. Rev. B* **14**, 200–207 (1976).
- Schlappa, J. *et al.* Direct observation of t_{2g} orbital ordering in magnetite. *Phys. Rev. Lett.* **100**, 026406 (2008).
- Chang, C. F. *et al.* Intrinsic and extrinsic x-ray absorption effects in soft x-ray diffraction from the superstructure in magnetite. *Phys. Rev. B* **83**, 073105 (2011).
- Tanaka, A. *et al.* Symmetry of orbital order in Fe₃O₄ studied by Fe $L_{2,3}$ resonant x-ray diffraction. *Phys. Rev. Lett.* **108**, 227203 (2012).
- Pontius, N. *et al.* Time-resolved resonant soft x-ray diffraction with free electron lasers: Femtosecond dynamics across the Verwey transition in magnetite. *Appl. Phys. Lett.* **98**, 182504 (2011).
- de Jong, S. *et al.* Speed limit of the insulator-metal transition in magnetite. *Nature Materials* **3718** (2013).



31. Goya, G. F., Berquo, T. S., Fonseca, F. C. & Morales, M. P. Static and dynamic magnetic properties of spherical magnetite nanoparticles. *J. Appl. Phys.* **94**, 3520–3528 (2003).
32. Poddar, P., Fried, T. & Markovich, G. First-order metal-insulator transition and spin-polarized tunneling in Fe₃O₄ nanocrystals. *Phys. Rev. B* **65**, 172405 (2002).
33. Özdemir, Ö. & Dunlop, D. J. Low-temperature properties of a single crystal of magnetite oriented along principal magnetic axes. *Earth and Planetary Science Letters* **165**, 229239 (1999).
34. Rezníček, R., Chlan, R., Štěpánková, H., Novák, P. & Maryško, M. Magnetocrystalline anisotropy of magnetite. *J. Phys.: Condens. Matter* **24**, 055501 (2012).
35. Crocombette, J. P., Thole, B. T. & Jollet, F. The importance of the magnetic dipole term in magneto-circular x-ray absorption dichroism for 3d transition metal compounds. *J. Phys.: Condens. Matter* **8**, 4095 (1996).
36. Perdew, J. P., Burke, K. & Ernzerhof, M. Generalized gradient approximation made simple. *Phys. Rev. Lett.* **77**, 3865–3868 (1996).
37. Goering, E. J., Lafkioti, M., Gold, S. & Schütz, G. Absorption spectroscopy and XMCD at the Verwey transition of Fe₃O₄. *J. Magn. Mater.* **310**, e249–e251 (2007).
38. Warland, A. *et al.* Effect of silica capping on the oxidation of Fe₃O₄ nanoparticles in dispersion revealed by x-ray absorption spectroscopy. *Phys. Rev. B* **85**, 235113 (2012).
39. van der Laan, G. Angular momentum sum rules for x-ray absorption. *Phys. Rev. B* **57**, 112–115 (1998).
40. Stöhr, J. Exploring the microscopic origin of magnetic anisotropies with X-ray magnetic circular dichroism (XMCD) spectroscopy. *J. Magn. Mater.* **200**, 470–497 (1999).
41. Ederer, C., Komelj, M., Davenport, J. W. & Fähnle, M. Comment on the analysis of angle-dependent X-ray magnetic circular dichroism in systems with reduced dimensionality. *J. Electron Spectrosc. Relat. Phenom.* **130**, 97–100 (2003).
42. Pellegrin, E. *et al.* Characterization of nanocrystalline γ -Fe₂O₃ with synchrotron radiation techniques. *Phys. Stat. Sol. (b)* **215**, 797–801 (1999).
43. Batlle, X. & Labarta, A. Finite-size effects in fine particles: magnetic and transport properties. *J. Phys. D: Appl. Phys.* **35**, R15–R42 (2002).
44. Warland, A. *Röntgenabsorptionsspektroskopie an Fe-Oxid-Nanopartikeln*. Doctoral thesis, University Duisburg-Essen (2013).
45. Darbandi, M. *et al.* Nanoscale size effect on surface spin canting in iron oxide nanoparticles synthesized by the microemulsion method. *J. Phys. D: Appl. Phys.* **45**, 195001 (2012).
46. Anisimov, V. I., Elfimov, I. S., Hamada, N. & Terakura, K. Charge-ordered insulating state of Fe₃O₄ from first-principles electronic structure calculations. *Phys. Rev. B* **54**, 4387–4390 (1996).
47. Anisimov, V. I., Zaanen, J. & Andersen, O. K. Band theory and Mott insulators: Hubbard *U* instead of Stoner *I*. *Phys. Rev. B* **44**, 943–954 (1991).
48. Blöchl, P. E. Projector augmented-wave method. *Phys. Rev. B* **50**, 17953–17979 (1994).
49. Kresse, G. & Joubert, D. From ultrasoft pseudopotentials to the projector augmented-wave method. *Phys. Rev. B* **59**, 1758 (1999).
50. Kresse, G. & Furthmüller, J. Efficient iterative schemes for *ab initio* total-energy calculations using a plane-wave basis set. *Phys. Rev. B* **54**, 11169–11186 (1996).

Acknowledgments

Fruitful discussions with C. Schüßler-Langeheine, F. M. F. de Groot and P. S. Miedema as well as support by E. Weschke and B. Klemke are gratefully acknowledged. We thank HZB for the allocation of synchrotron radiation beamtime. Funded by BMBF (05 ES3XBA/5) and DFG (WE2623/3-1). We are grateful to NSC under Swedish National Infrastructure for Computing (SNIC) and the PRACE-2IP project (FP7 RI-283493) resource Abel supercomputer based in Norway at University of Oslo for providing computing facility. B.S. acknowledges VR Swedish Research Links programme and Carl Tryggers Stiftelse for financial support. O.E. acknowledges support from the eSENCE, VR, KAW foundation and the ERC.

Author contributions

D.S. and C.S.A. performed the measurements, the data evaluation and wrote the manuscript, A.W. performed the XMCD measurements, M.D. prepared the nanoparticles, S.H. and S.B. performed the calculations, O.E. and B.S. wrote the theoretical part of the manuscript, and H.W. wrote the manuscript.

Additional information

Supplementary information accompanies this paper at <http://www.nature.com/scientificreports>

Competing financial interests: The authors declare no competing financial interests.

How to cite this article: Schmitz, D. *et al.* The dipole moment of the spin density as a local indicator for phase transitions. *Sci. Rep.* **4**, 5760; DOI:10.1038/srep05760 (2014).



This work is licensed under a Creative Commons Attribution-NonCommercial-NoDerivs 4.0 International License. The images or other third party material in this article are included in the article's Creative Commons license, unless indicated otherwise in the credit line; if the material is not included under the Creative Commons license, users will need to obtain permission from the license holder in order to reproduce the material. To view a copy of this license, visit <http://creativecommons.org/licenses/by-nc-nd/4.0/>